Three-Pulse Photon-Echo Peak Shift Spectroscopy and Its Application for the Study of Solvation and Nanoscale Excitons

ARTICLE *in* CHEMPHYSCHEM · JANUARY 2011

Impact Factor: 3.42 · DOI: 10.1002/cphc.201000712 · Source: PubMed

4 AUTHORS, INCLUDING:

Megan Oh
University of Toronto
8 PUBLICATIONS **244** CITATIONS

SEE PROFILE

CHEMPHYSCHEM

DOI: 10.1002/cphc.201000712

Three-Pulse Photon-Echo Peak Shift Spectroscopy and Its Application for the Study of Solvation and Nanoscale Excitons

Megan H. J. Oh, Mayrose R. Salvador, Cathy Y. Wong, and Gregory D. Scholes*[a]

An understanding of chemical reactivity begins with an understanding of the dynamics involved regarding system–bath interactions. Spectroscopic studies of these interactions in condensed-phase multichromophoric systems are intricate and contain much information. Photon-echo spectroscopy has proven to be a useful tool for probing these interactions. A description of three-pulse photon-echo peak shift spectroscopy (3PEPS)—theory, experiment, and application—for the study of solvation and dynamics of nanoscale excitons is presented. Also, we discuss how two-dimensional photon-echo spectroscopy (2DPE) relates to 3PEPS and show how 3PEPS data can be extracted from 2D photon-echo data.

1. Introduction

The condensed-phase spectroscopy of molecules, conjugated polymers, multichromophoric dendrimers, photosynthetic proteins, and numerous other systems of interest is characterized by broad absorption and fluorescence lineshapes where practically all of the vibronic details are lost. Therefore, unlike high-resolution spectroscopy or sub-ensemble methods, linear frequency domain ensemble techniques tend to yield limited information for complex condensed-phase systems. As a consequence there has been much effort over the past decades directed to the development of nonlinear optical spectroscopies.

As an example, Figure 1[1] shows a visible absorption spectrum for 1,2,4,5-tetrazine at room temperature in the vapour phase and in two other condensed phases (hexane and aqueous solutions). In the vapour phase, a series of sharp peaks resulting from the superposition of vibrational transitions over the electronic transitions can be seen. In the solvents, these fine structures are reduced or eliminated due to interaction between the chromophore and the bath (i.e. solvent modes couple to the solute) and much of the dynamics become masked. Nonetheless, there is a wealth of information in condensed-phase spectra. It is important to extract that information to elucidate more deeply, for example, how reaction rates are influenced by solvation, the mechanism of fundamental reactions such as energy, electron, and proton transfers, or to understand the limits imposed on wavefunction delocalization in complex multichromophoric systems.

Herein we review recent applications of a nonlinear optical spectroscopy called three-pulse photon-echo peak shift (3PEPS) in condensed-phase spectroscopy. We describe how the method works, what has been learned from its application, and how it is related to two-dimensional photon-echo spectroscopy.

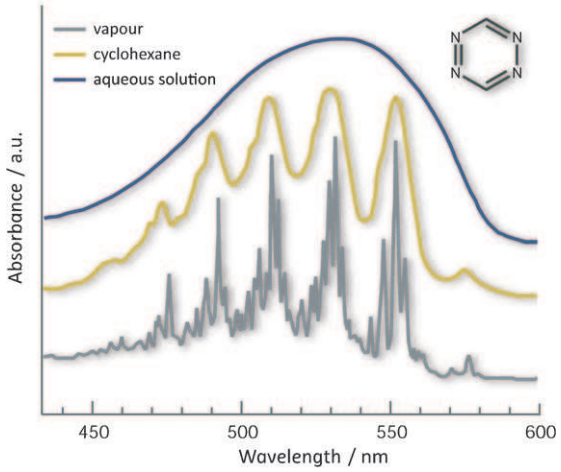

Figure 1. Visible absorption spectrum of 1,2,4,5-tetrazine at room temperature in the vapour phase, in a hexane solution, and in an aqueous solution. The vibronic fine structure observed in the gas phase is lost in the solution state (condensed phase).

2. Background on Condensed-Phase Spectroscopy

2.1. Molecules Interact with Their Environment

The energy of the absorption and fluorescence band maxima of many molecules depends on the solvent; a phenomenon called solvatochromism. Solvatochromism arises because the ground and excited electronic states interact slightly differently with the solvent. For example, in the case of dipolar solvation, a change in dipole moment upon photoexcitation can be caused by the change in electron distribution in the molecule.

[a] *M. H. J. Oh, M. R. Salvador, C. Y. Wong, Prof. G. D. Scholes*
Department of Chemistry, Institute for Optical Sciences
University of Toronto
80 St. George Street, Toronto
Ontario M5S3H6 (Canada)
Fax: (+1) 416-978-8775
E-mail: gscholes@chem.utoronto.ca

Naturally, the strength of the net coulomb interaction between the dipole and the surrounding solvent molecule (ground-state) dipole moments will be affected. This, and other effects that influence the spectrum, were quantified in important early papers by Ooshika,[2] McRae,[3] Mataga,[4] and Lippert.[5] There are a number of useful recent reviews including those by Suppan,[6] Tomasi,[7] Cramer,[8] and Reichardt.[9]

In the systematic treatment described by Marcus,[10] the solute is separated from all other degrees of freedom (the medium, solvent, or bath). Then the functional dependence of solute–medium interactions on the permanent and induced charge distributions are determined. In the process, an appropriate statistical–mechanical distribution of the fluctuating coordinates is accounted for (the medium is not static or ordered). Assuming that polar interactions dominate the solvation, it is found that the free energy change of the system in response to the solute making an electronic transition from $|i\rangle$ to $|f\rangle$ at temperature T is [Eq. (1)]:

$$\Delta E(T) = F_f - F_i + F^{op}_{f-i} - F_{f-i} \quad (1)$$

It is assumed that the $i \rightarrow f$ transition occurs at fixed nuclear configuration corresponding to the equilibrium distribution for $|i\rangle$. Here, F_f and F_i are polar contributions to the Helmholtz free energy of a system in which the solute is in its final and initial electronic states, respectively. F_{f-i} is the corresponding contribution for a theoretical solute, the permanent charge distribution of which is that of the final state minus the initial state, and F^{op}_{f-i} is the polar contribution to the free energy in which the medium responds to the $f-i$ charge distribution only through an optical polarization. Marcus further argues that the fixed-volume condition can be replaced by the approximate equality of change in Helmholtz free energy and Gibbs free energy. This permits a more accurate representation of the medium response.

In the case of absorption, $|i\rangle$ is the ground electronic state that we label g, and $|f\rangle$ is the excited state e. Equation (1) is rewritten as Equation (2):

$$\Delta E^{abs}(T) = F_e - F_g + \lambda \quad (2)$$

where $\lambda = F^{op}_{f-i} - F_{f-i}$. It is the reorganization energy associated with a change in medium configuration to equilibriate e. Similarly, an expression can be derived for fluorescence [Eq. (3)]:

$$\Delta E^{flu}(T) = F_e - F_g - \lambda \quad (3)$$

The significance of these quantities can be understood by plotting the free energy, ΔF (which we have equated to ΔG), versus the generalized bath coordinate (or net medium polarization) Q (Figure 2).

These free energy curves have a Gaussian shape (quadratic dependence on Q) if we assume linear response (vide infra). It is evident that the $F_e - F_g$ term in Equation (2) lowers one curve with respect to the other, while λ arises owing to translation of one curve with $\langle Q \rangle$. It can furthermore be gathered from inspection of Figure 2 that the Stokes shift, the difference in energy between the absorption and fluorescence maxima, is equal to 2λ.

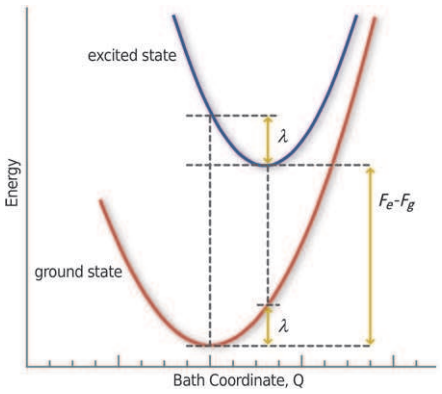

Figure 2. Schematic representation of the energetics of electronic transitions in a chromophore in a polarizable medium. The x-axis, Q, is a generalized bath coordinate describing the orientation and polarization of surrounding dipoles in the medium.

The quantities in Equations (2) and (3) can be quantified by modeling each electronic state as a polarizable (α) point dipole (μ) in a spherical cavity of radius a that is surrounded by solvent. Then ΔE^{abs} and ΔE^{flu} are [Eqs. (4) and (5)]:

$$\Delta E^{abs}(T) \approx -\left[f^{op}\left(\mu_e^2 - \mu_g^2\right) + (f - f^{op})\mu_g(\mu_e - \mu_g)\right] \quad (4)$$

$$\Delta E^{flu}(T) \approx -\left[f^{op}\left(\mu_e^2 - \mu_g^2\right) + (f - f^{op})\mu_e(\mu_e - \mu_g)\right] \quad (5)$$

where [Eq. (6)]:

$$f = \frac{1}{a^3}\left[\frac{2(D-1)}{2D+1}\right] \quad (6)$$

and [Eq. (7)]:

$$f^{op} = \frac{1}{a^3}\left[\frac{2(n^2-1)}{2n^2+1}\right] \quad (7)$$

D is the static dielectric constant of the solvent and n is the refractive index.

2.2. Interaction Timescales are Important

There are countless solvent configurations around a molecule in solution, although many different configurations will have similar energies. This is embodied in the generalized coordinate Q (Figure 2). Assuming that these solvent configurations are independent random variables, then they will be normally distributed according to the central limit theorem (i.e. the statistics are Gaussian). Then, assuming that the molecule is linearly coupled to the solvent, we obtain the quadratic free energy curves plotted in Figure 2.

Why are electronic lineshapes (ignoring vibronic transitions for simplicity) not usually Gaussian? The reason is that the solvent configurations are continually changing over a range of timescales. If those changes are very slow, then the lineshape

will be Gaussian, a limit known as inhomogeneous broadening. Experimentally, the range of environments occupied by the molecules within an ensemble can be deduced from spectral hole burning or single-molecule spectroscopy.[11–13] In the limit that the solvent fluctuations are extremely fast, the lineshape is Lorenzian[14] and the Stokes shift is nonexistent. Usually, however, the fluctuations occur on some intermediate timescale and there are correlations from one solvent configuration to another.[15] The correlation function that describes the transition energy fluctuations [Eq. (8)]:

$$M(t) = \frac{\langle \delta E(t) \delta E(0) \rangle}{\langle \delta E^2 \rangle} \tag{8}$$

represents the time-development of the Stokes shift.[16,17] This function can be determined from 3PEPS measurements. More generally, this function is important for many nonlinear optical spectroscopies in the condensed phase.[14,18–20] For example, there is a Fourier relationship between this correlation function and the spectral line shape [Eq. (9)]:

$$\sigma(\omega) = \frac{1}{\pi} \int_0^\infty dt M(t) \exp(-i\omega t) \tag{9}$$

The first observation of the correlation function of Equation (8) was achieved by monitoring the time-dependent Stokes shift and the reader should refer to refs. [21–23] for details of those important experiments. There are also some excellent reviews that provide more detailed discussions than we pursue herein.[24–31]

2.3. Fluctuations Give Linewidth and the Stokes Shift

The solvent fluctuations are stochastic, yet they allow relaxation to an equilibrated free energy; that is the dynamic Stokes shift. The random fluctuations of the medium are influenced by the solute, and microscopically, it is the Bose–Einstein statistics of phonon occupation that provide the tendency for the system to equilibrate.

The transition energy fluctuations are closely related to the Stokes shift, as can be deduced from Equations (2) and (3). More formally this relationship can be expressed as a fluctuation-dissipation theorem,[32] revealing a general relationship between the response of a given system to an external disturbance and the internal fluctuations of the system in the absence of the disturbance. Hence the mean-square fluctuation in energy difference between $|g\rangle$ to $|e\rangle$ (closely related to the homogeneous line broadening) is directly related to the Stokes shift given in Equation (10):

$$\delta^2 = 2kT\lambda \tag{10}$$

where T is temperature and k is the Boltzmann constant.

Finally, it is worth noting that intermolecular forces play a role in the ultrafast contributions to the dynamic Stokes shift.[33] The result is an initial Gaussian decay of $M(t)$ called the inertial solvent response.[34–39] When a molecule is transferred to an excited electronic state by photoexcitation, many of the vibrational modes of the molecule as well as those for solute–solvent librational modes instantaneously change their equilibrium coordinates because the molecule has a slightly different equilibrium geometry in the excited state compared to the ground state. The inertial solvation response is the equilibration of the zero-point motions of these modes.

3. Three-Pulse Photon-Echo Peak Shift (3PEPS)

3PEPS is a nonlinear optical spectroscopy that can measure the timescales of dephasing and the strengths of chromophore–bath interactions. This technique takes advantage of the fact that following excitation, the resonant transition frequencies of an inhomogeneous ensemble of chromophores each carries a phase factor in the time-domain representation that spreads the transition frequencies during a coherence time. In a photon-echo experiment, that spread—and hence the inhomogeneous line broadening—can be canceled by the pulse sequence. That rephasing capability of the photon-echo experiment, however, is limited by a stochastic spread of the frequencies that can, for example, be caused by the coupling of the energy gap to solvent molecules and intramolecular modes. The peak shift essentially records the rephasing capability of the photon-echo pulse sequence as a function of spectral diffusion time and thereby measures the timescales of the environment that cause homogeneous dephasing.

In the 3PEPS measurements the signal arising from the third-order nonlinear optical polarization, $P^{(3)}(t)$, is measured as a function of the delay between the first and second pulses (τ) and the delay between the second and third pulses (T). In a two-electronic state picture, the first pulse is used to create a coherent superposition of the ground $|g\rangle$ and the excited state $|e\rangle$ oscillating at a frequency corresponding to their energy difference. During the time period τ, referred to as coherence time, the response of the system to the perturbation modulates the transition frequency $\omega_{eg} = \omega_e - \omega_g$. When the second pulse is applied, a population in the excited or ground state is created. This period is called the population time (T). At short T periods, the memory of the initial distribution of the transition frequency is stored. As T increases, the molecules can begin to explore the range of transition frequencies available to them, resulting in a loss of memory of the initial distribution. This is also known as spectral diffusion. The third pulse is used to initiate the rephasing, in which case, a photon-echo signal is radiated and it peaks at $t > 0$ if the system remembers its initial transition frequency. On the other hand, if the memory is lost, as in the case of long T, the echo will peak at $t = 0$. The term rephasing is used when the coherence created after the third pulse is a Hermitian conjugate of the coherence created after the first pulse.

The characteristic of rephasing pathways of a photon-echo signal is that the first time delay τ involves the coherence $|g\rangle\langle e|$, while the complex conjugate coherence $|e\rangle\langle g|$ evolves during the final time period t, where g labels the ground electronic state and e an excited electronic state. Initially, the en-

semble of molecules is forced to undergo electronic oscillation at the laser frequency. Then, during the time interval τ, each transition returns to its natural oscillation frequency defined by the energy of the ground to excited-state transition. At some time all the electronic oscillations in the ensemble have different enough frequencies that the radiated polarizations interfere destructively on a detector, giving no measured signal. What happens during the rephasing time period $t>0$ is that the evolution of the natural frequency of the oscillators is reversed. An electronic phase defined as $\phi(t)=\omega_{\alpha\beta}t$ (where $\omega_{\alpha\beta}=(E_\alpha-E_\beta)/\hbar$) associated with the oscillating terms $\exp(-i\omega_{\alpha\beta}t)$ in the equations describing the signal, is accumulated during the coherence time τ, then reversed during the final time period t. Therefore, at a time $t=\tau$ all the electronic oscillators are in phase, they interfere constructively on the detector and a signal is seen. The measured signal intensity appears to radiate at some delay after the final excitation pulse. Really, the molecules are each radiating continuously after the last pulse, but the fields are only in phase at time $t=\tau$.

The decay of the peak shift as a function of T can be used to study fast (tens of femtoseconds) and slow (over hundreds of nanoseconds) nuclear fluctuations leading to memory loss.[40,41] The timescales of these fluctuations can give insight to their origins. In order to achieve this, the fluctuations of the transition energy gap in Equation (11) [the time-dependence of the energy gap], recorded through the 3PEPS measurement:

$$\omega_i(t)=\langle\omega\rangle+\delta\omega_i(t)+\varepsilon_i \tag{11}$$

is used to define a correlation function, Equation (8), for the fluctuating portion of Equation (11), where $\delta\omega=\delta E/\hbar$.

In Equation (11), $\langle\omega\rangle$ is the average electronic transition frequency of the ensemble, $\delta\omega_i(t)$ is the dynamical fluctuation term, and ε_i is the static offset of the chromophore from the ensemble average.[15] The correlation function of the fluctuations (of the normalized transition energy gap), also known as the solvation dynamics in the echo signal, is contained within $M(t)$. This correlation contains all information needed to completely describe the optical response of the system, therefore once $M(t)$ is known, it can be used to determine the lineshape function, $g(t)$. The lineshape function is defined as [Eq. (12)]:

$$g(t)=-i\lambda\int_0^t dt_1 M'(t_1)+\langle\delta\omega^2\rangle\int_0^t dt_1\int_0^{t_1} dt_2 M''(t_2) \tag{12}$$

where λ is the reorganizational energy of the bath, $\langle\delta\omega^2\rangle^{1/2}$ is the coupling strength, and $M'(t)$ and $M''(t)$ are given by Equations (13) and (14):

$$M'(t)=\frac{1}{\pi\Delta^2}\int_0^\infty d\omega\tilde{C}(\omega)\coth\left(\frac{\beta\hbar\omega}{2}\right)\cos(\omega t) \tag{13}$$

$$M''(t)=\frac{1}{\pi\lambda}\int_0^\infty d\omega\frac{\tilde{C}(\omega)}{\omega}\cos(\omega t) \tag{14}$$

with [Eqs. (15) and (16)]:

$$\Delta^2=\frac{1}{\pi}\int_0^\infty d\omega C''(\omega)\coth\left(\frac{\hbar\omega}{2k_BT}\right) \tag{15}$$

$$\lambda=\frac{1}{\pi}\int_0^\infty d\omega\frac{C''(\omega)}{\omega} \tag{16}$$

Equations (13) and (14) show the relationship between the correlation function and the spectral density $C(\omega)$. The contributions to $M(t)$ include intramolecular vibrational motions and system–bath dissipative processes (fluctuations of the bath). It is usually difficult to separate these processes. If $g(t)$ is known, however, the coupling of the nuclear motion to the bath can be explained. The 3PEPS experiment gives us the information that is contained in the three-pulse photon-echo (3PE) signals in a condensed form (Figure 3). Simulations are performed to obtain the correlation function and insights into $g(t)$.[18,42]

3PEPS data are plotted as peak shift (τ^*) versus population time (T) and thus provide the correlation function for the electronic energy gap of the probe molecule. From the data, the characteristic timescales of bath relaxation and the coupling strength of the bath to the probe molecule can be obtained.[40,43] Also, inhomogeneous line broadening can be determined.

In a general overview of the 3PEPS plot features, a nonzero asymptotic peak shift is characteristic of disorder in the system (inhomogeneous broadening in linear spectroscopy), as the memory of the initially prepared state is retained by the system. The peak shift reports on the timescale of homogeneous line broadening and is influenced by experimental conditions such as pulse width. Typically, a higher initial peak-shift value corresponds to a weaker system coupling to the bath (electron–phonon coupling) and therefore decreased homogeneous broadening. Increasing the bath coupling (λ) will change the value of the asymptotic peak shift, and more significantly, it will reduce the initial peak shift. Additionally, the damped oscillations seen in the data can be attributed to intramolecular vibrations.

The peak shift decays as $M(t)$ in the absence of static inhomogeneity. The peak-shift dependence on population time can be understood using the following approximate equation for the asymptotic peak shift [Eq. (17)]:[43]

$$\tau^*(T\to\infty)=\frac{\sigma_{in}^2\sqrt{\Gamma+\sigma_{in}^2+\lambda^2}}{\sqrt{\pi}[\Gamma(\Gamma+\sigma_{in}^2+\lambda^2)+\sigma_{in}^2\lambda^2]} \tag{17}$$

where $\Gamma=2\lambda/(\hbar\beta)$, $\beta=1/kT$, and λ is the total reorganizational energy divided by $\hbar$. In the long time limit, the peak shift decays to zero when Equation (17) equals zero. When the equation does not equal zero, a nonzero peak shift is observed. Figure 4[42] shows a typical example of 3PEPS data. The 3PEPS data was simulated using an exponential $M(t)$, systematically static disorder was introduced and bath coupling was modified to show their effects on $M(t)$. It can be seen from

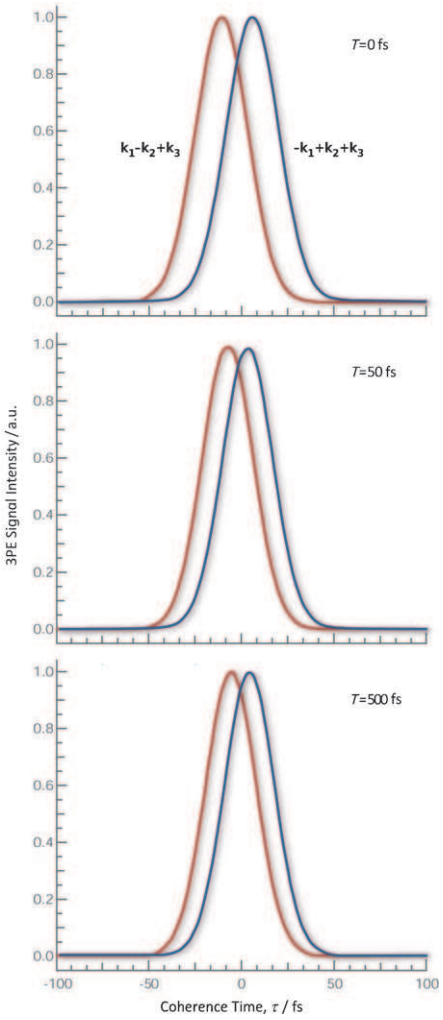

Figure 3. Typical normalized time-integrated 3PE profiles (Gaussian fits only, data points omitted) in the two phase-matching directions $\mathbf{k}_1-\mathbf{k}_2+\mathbf{k}_3$ (red line) and $-\mathbf{k}_1+\mathbf{k}_2+\mathbf{k}_3$ (blue line) for various population times *T*. The signals are fitted to a Gaussian and the peak shift τ^*, for each population time *T*, corresponds to the middle of the peak-to-peak distance of the time-integrated photon-echo signals.

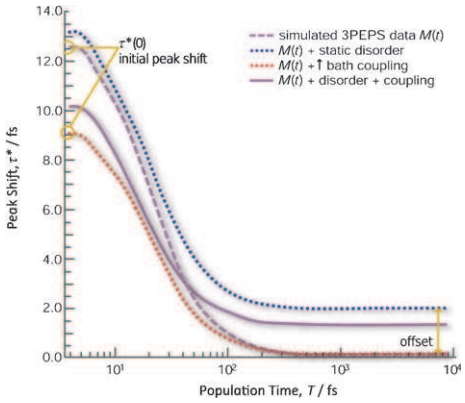

Figure 4. Typical example of 3PEPS data. Simulated 3PEPS data (purple dashed line) using an exponential *M*(*t*). Disorder in the system is introduced by adding a static Gaussian contribution to the same *M*(*t*) term (blue dotted line). An asymptotic peak shift or offset at long population times is now evident. The effect of the strength of bath coupling can also be simulated by increasing/decreasing the coupling value in the *M*(*t*) expression. One of the effects of increased coupling is a decrease in the initial peak shift (red dotted line). Incorporating the disorder into the system, as well as increasing the coupling strength results in a decreased initial peak shift and an asymptotic offset (purple solid line).

Figure 4 that incorporating static disorder as well as increasing the bath coupling strength in the simulation results in a lowered initial peak shift and a manifestation of a nonzero peak shift at long population times.[18,43]

The above formalism was made by considering a two-level system. However, for more complicated multichromophoric and excitonic systems, a general two-level system becomes insufficient to interpret the experimental results. In this case, it may be necessary to use a three- or higher-level system to model the results.[44]

3.1. The Experiment

In a 3PEPS experiment a sweep of the coherence time (τ) is made for a fixed value of the population time (*T*). The population time is then incremented to a new value and the coherence time is swept again. A three-dimensional surface is effectively recorded where the signal is dependent on the two independent variables τ and *T*. The quantity of interest from the signal is the peak shift (τ^*), defined as the time of the maximum signal along the coherence delay for a fixed value of the population time.

Experimentally, we carry out the procedure as follows. Two beams are independently delayed using retroreflectors mounted on motorized delay stages. Pulse delays are scanned from negative τ (pulse sequence 2–1–3) to positive τ (pulse sequence 1–2–3), such that the population time *T* is fixed between pulses 1 and 3 at $\tau<0$ and then between 2 and 3 at $\tau>0$. The three *S*-polarized beams are aligned after the delay stages to form an equilateral triangle beam geometry (with sides of 1 cm)[45] and are focused into the sample using a silver-coated spherical mirror ($f=25$ cm). The 3PE signals in the $-\mathbf{k}_1+\mathbf{k}_2+\mathbf{k}_3$ and $\mathbf{k}_1-\mathbf{k}_2+\mathbf{k}_3$ phase-matching directions are spatially isolated using irises and measured simultaneously using diodes (10 ns rise time) and lock-in detection. Each of the phase-matching signals is approximately symmetric and its maximum is shifted from the $\tau=0$ position. The signals are fitted to a Gaussian and the peak shift, τ^*, for each population time, *T*, corresponds to the average of the coherence time when the time-integrated photon-echo signals peak (i.e. half of the peak to peak distance between the two signals or Gaussian fits), Figure 3. The temporal overlap between the three pulses is set initially by autocorrelating each of the three pulse pairs. Accurate $T=0$ and $\tau=0$ stage positions are set according to overlap of the pulses in the sample by measuring all three three-pulse echo signals and using the symmetry of the echo signals along the τ time axis. The time delay between pulses 1 and 2 is set using $-\mathbf{k}_1+\mathbf{k}_2+\mathbf{k}_3$ and $\mathbf{k}_1-\mathbf{k}_2+\mathbf{k}_3$ signals. The delay between pulses 2 and 3 is set using the $-\mathbf{k}_1+\mathbf{k}_2+\mathbf{k}_3$ and $\mathbf{k}_1-\mathbf{k}_2+\mathbf{k}_3$ signals.

3.2. Pulse Duration and Overlap Issues

The solvation correlation function has been identified as a central parameter of interest for dynamical processes in the condensed phase. In 3PEPS, the peak shift as a function of T is observed and is approximately proportional to the time correlation function, $M(t)$, of the electronic transition energy for population times longer than 50–100 fs (under the impulsive limit and assuming that nuclear dynamics are classical) [Eq. (18)]:[40,43,46,47]

$$\bar{\tau}(T) \approx \sqrt{\frac{\beta\hbar}{2\pi\lambda}} M(T) \tag{18}$$

with $\beta = 1/k_B T_K$, where k_B is the Boltzmann constant and T_K is the absolute temperature. One problem associated with the 3PEPS method is its inability to characterize entirely the initial decay of $M(t)$. Thus, for short times of T, 3PEPS cannot distinguish between the different types of system–bath interactions (i.e. the Kubo or the multimode Brownian oscillator model because $M(t)$ is obscured by other signals caused by pulse overlap).[15] For the determination of the short-time solvation dynamics by this experiment, the extraction involves a rather complex and tedious nonlinear fitting procedure.[18,48–50] However, Everitt et al. have proposed another relatively simple approach, S3PE (slope of the three-pulse echo) method, which would allow for the extraction of the time correlation function for all times.[47] In S3PE, a series of slopes of the echo signal as a function of T, $\bar{S}(T)$, are determined. The normalized slopes, $S(T)$, given in Equation (19), are directly equivalent to the normalized time correlation function of the transition energy, applicable over all times of T (under the same limit and assumption as the 3PEPS method):[46,47,51]

$$S(T) \equiv \frac{\bar{S}(T)}{\bar{S}(0)} \approx M(T) \tag{19}$$

Another approach exists, in addition to S3PE, which appears to give more accurate determination of the initial curvature of the solvation correlation function. However it requires a time-gated experiment and more analysis beyond the simplistic S3PE approach.[47] It should also be noted that both methods are based on the assumption that the frequency fluctuations are Gaussian.

Real pulses are of finite duration, so overlap of the three pulses will occur in the region of $\tau = T = 0$. The finite duration of pulses induces an asymmetric shape of the time-integrated signal, especially at short population times T.[46,47] Since both methods are measured by fitting the echo signal with a symmetric Gaussian function, this approximation hampers an accurate extraction of the time correlation function.[40,47,52–54]

In S3PE, when the pulse duration is finite, difficulties arise due to discontinuous slopes of the signals for short T. The discontinuity disappears as T becomes greater than the pulse duration. However, due to such discontinuity (regardless of how short the pulse width is compared to the timescales of the solvation), the advantage of the S3PE approach over the 3PEPS method found in the impulsive limit, is significantly diminished. This is especially because 3PEPS appears to be a better match for the time correlation function at longer times for the finite pulse duration.[18,47,55] The S3PE method could potentially be a useful approach, however, as long as pulse durations are short compared to the timescale of transition-frequency fluctuations, the impulsive limit generalization can be used, and the 3PEPS observables and determination of the solvation correlation function are not significantly affected by the effects of the finite pulse.

In 3PEPS, the experimental peak-shift values, obtained by Gaussian fitting, are smaller than the predicted peak-shift values at early times of T.[54] With the introduction of the partial Gaussian fitting method, for positive values of τ by Larsen et al.,[52] and a different scanning method, which switches the roles of the pulses 1 and 2 introduced by Wiersma et al.,[40] the short time errors caused by the Gaussian approximation can be minimized and a more symmetric shape of the signal can be obtained.[46] This will lead to more accurate peak-shift data and short time solvation dynamics by minimizing the ramifications of the finite pulse and fitting approximation.

4. Application to Multichromophoric and Excitonic Systems

The advantages of 3PEPS have been discussed in much detail, and owing to these efforts, many researchers view it as an essential tool for the investigation of environmental fluctuation dynamics around a chromophore. 3PEPS enables us to retrieve a generalized picture related to spectral diffusion and timescales of processes contributing to spectral line broadening (elucidating the line shapes of linear absorption and fluorescence spectroscopies) or changes in the microscopic nature of the excited state (e.g. energy transfer, excitation localization, etc.). The relative simplicity of the approach has inspired investigations in many complex multichromophoric and excitonic systems, such as semiconductor nanocrystals, conjugated polymers, dendrimers, and single-walled carbon nanotubes, as is highlighted next.

4.1. Semiconductor Nanocrystals

It is well known that semiconductor quantum dots (QDs) exhibit size-dependent optical properties owing to strong confinement of their excitons. These optical properties can be studied by controlling the transient nonlinear response initiated by ultrafast optical pulse sequences (i.e. photon-echo spectroscopies). In a previous study, we measured the homogeneous (due to coupling of electronic transition to nuclear motion) and inhomogeneous (due to distribution of quantum dot sizes) broadening contribution to the absorption spectrum of CdSe nanocrystals.[56]

In our results, two CdSe samples of the same average size but of different size distributions were compared. In Figure 5, the 3PEPS data for the two CdSe samples and a simple two-level and non-inhomogeneously broadened model system, Rhodamine 6G (R6G), are shown. It is apparent that while the

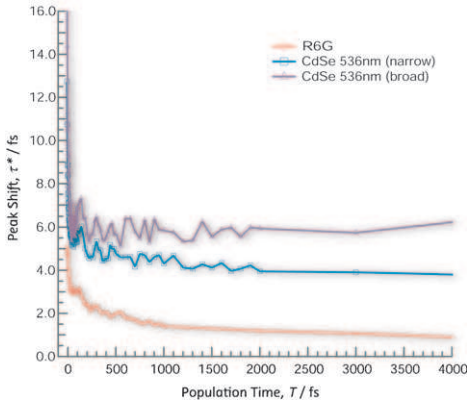

Figure 5. 3PEPS data collected for CdSe quantum dot samples (with lowest exciton band absorption maxium at 536 nm) having a broad size distribution (triangles), having a narrow size distribution (squares), and Rhodamine 6G in ethanol (circles).

R6G peak shift goes to zero at sufficiently long population times, the CdSe samples tend to a nonzero asymptotic value in each case. The long-time peak-shift offset for the sample with a broader size distribution is higher in comparison to the sample with a narrower size distribution. This offset, indicative of the static inhomogeneity of the system, is caused by a static distribution of energy gaps resulting from the nanocrystal size distributions.

3PEPS data is able to capture a great dynamic range, from femtoseconds to nanoseconds, of detailed information on a wide range of nuclear motions that couple to an electronic transition. Quantification of this information is possible by simulating the data using a general model for the electronic transition frequency of an individual quantum dot. From the simulations, it was found that the homogeneous broadening arises from Gaussian (inertial), exponential/Debye (Kubo) and vibrational coupling of the nanocrystal to the bath, which is mainly comprised of the capping trioctylphosphine oxide (TOPO) ligands. Size-dependence data showed that the surface has an important role in the relaxation of the nanocrystals when probed optically. Larger nanocrytals have longer Gaussian relaxation times when compared to smaller nanocrystals.

A recent investigation by McKimmie et al.[57] used 3PEPS to explore how the various capping materials and the capping process affects the phonon modes and ultrafast dynamics of QDs. Their study on QDs with a CdSe core and various capping materials (–CdS, –CdS–ZnS, –CdS–CdZnS–ZnS) showed that capping layers play an important role in the inherent ultrafast dephasing characteristic of the samples. This is because the capping layers affect not only the optical properties, but also the morphology of the nanocrystals. The changes in the optical properties are due to the varying degrees to which electron and hole wave functions can seep into the different types of shells. For example, ZnS (a material with a larger bandgap than CdS) can provide stronger carrier localization than CdS (a material with a larger bandgap than CdSe) when deposited onto a CdSe core, hence a higher ZnS content shelling produces a smaller carrier delocalization and is red-shifted less in the absorption spectrum of the original CdSe QD compared to the CdS shell. Morphological changes are induced through capping of the core material as well. For example, capping of the CdSe core (originally spherical) with a –CdS–ZnS shell forms nonspherical, stunted, bullet-shaped nanocrystals (aspect ratio 1:1.4) with a slightly broader size distribution compared to the other samples (capping with –CdS and –CdS–CdZnS–ZnS maintains the original spherical shape).

In their 3PEPS study, when they compared the peak shifts of the three samples, they found that CdSe–CdS samples, which maintained highly spherical and monodisperse QDs, had the smallest peak shift (suggesting a small distribution of transition frequencies). The CdSe–CdS–CdZnS–ZnS sample, QDs of which were also spherical with a slightly larger diameter and size distribution compared to the CdSe–CdS sample, also had a small peak shift (slightly larger than the CdSe–CdS sample), while the CdSe–CdS–ZnS sample showed a considerable increase in peak shift compared to the rest, resulting from a larger distribution of transition frequencies due to the asymmetry in its morphology. For phonon modes, the vibrational quantum beat frequency of the 3PEPS simulations, resulting from the longitudinal optical (LO) phonons, seemed independent of the capping layer, indicating that the CdSe core had a greater influence on the behaviour of the excited state of the QD than the capping layers. The experimentally observed frequencies for the longitudinal acoustic (LA) phonon mode were virtually the same for the core/shell samples, but the damping time of the LA phonon was shown to be dependent on the morphology and uniformity of the sample.

From these studies we are able to see that inhomogeneous broadening is a consequence of size distribution. Size-, capping-layer-, and morphology-dependent optical properties of QDs were clearly evident and a stronger than anticipated exciton–bath coupling was observed. It was also shown that 3PEPS spectroscopy can quantify these contributions to QD optical spectroscopy.

4.2. Conjugated Polymers

The non-mirror-image absorption and emission spectra of conjugated polymers may be the result of various dynamic contributions which can be complicated to discern. 3PEPS spectroscopy is able to probe the early time dynamics that are often obscured by ensemble averaging of linear spectroscopy and quantify the ultrafast dynamics involved in the evolution of excitations in conjugated polymers. Dykstra et al.[58] in their investigation of the origins of line broadening and excited-state dynamics for a conjugated polymer (MEH-PPV) and a model oligomer demonstrated how 3PEPS can be utilized to elucidate dephasing mechanisms, spectral inhomogeneity arising from conformational disorder, and dynamical processes within the system.

The conjugation and conformational disorder that occur within a conjugated polymer chain are expected to play an important role in its optical properties and distinguish these systems from molecular dyes and inorganic semiconductors.[58–70] The absorption and emission spectra of MEH-PPV and a model

oligomer show similar features, in that they both have broad, unstructured absorption bands and narrow, structured emission spectra. At first glance, the similarities suggest that the main origins of line broadening do not differ as much as expected, even though there is a stronger static inhomogeneity contribution predicted in the conjugated polymer, reflecting the inherent conformational disorder.[58]

In a qualitative analysis of the 3PEPS result, it was found that the conjugated polymer had a higher asymptotic offset compared to the oligomer. Conformational disorder in such a system is observed as a nonzero asymptotic peak shift. The measure of the nonzero persistent peak shift was associated with the degree of structural defects along the conjugation backbone. Damped oscillations in the data were also observed for both the oligomer and the conjugated polymer. These oscillations were attributed to coherently excited intramolecular vibrations that were weakly damped by the bath. However, in the conjugated polymer, the oscillations were diminished by many averaged excited vibrational modes of the various-sized conformational subunits. In addition, both systems showed a high initial peak shift indicating a weak coupling to the bath.

In order to obtain a consistent physical picture for the ultrafast dynamics of excitons in conjugated polymers after photoexcitation, as well as to account for the observed Stokes shift, simultaneous modeling of the 3PEPS, absorption, and fluorescence data were carried out. From this, a phenomenological model was proposed which states that absorption occurs from the ground state to a delocalized set of states steming from the electronic coupling between conformational subunits and that this set of states appears as inhomogeneous broadening in the absorption spectrum. Photoexcitation of the conjugated polymer produces a highly nonequilibrium geometry, and upon subsequent relaxation, the strong coupling of electronic transitions to the nuclear coordinate promotes rapid localization of the excitation. This relaxation was monitored by 3PEPS as a type of spectral diffusion (manifested as a rapid peak-shift decay on a timescale of ~25 fs). Through this investigation, a better insight into disorder and exciton dynamics in MEH-PPV and other conjugated polymers was obtained.

More recent studies using two-dimensional photon-echo spectroscopy and a technique called two-time anisotropy decay have revealed that the ultrafast exciton relaxation processes in MEH-PPV are accompanied by complex quantum-coherent dynamics.[71]

Wells et al.,[72] recently reported two-colour 3PEPS measurements of the initial exciton dynamics in another type of conjugated polymer, poly(3-hexylthiophene) (P3HT). In their results, they observed a preservation of energetic correlation during the large ultrafast spectral migration, which indicates that the initial exciton relaxation is driven by selective exciton–phonon coupling to torsional motions and is not primarily a stochastic localization process. Hence, two-colour 3PEPS provides more insight into spectral diffusion because it allows one to observe whether or not spectral diffusion is correlated across a frequency distribution.[73]

4.3. Branched or Dendrimeric Macromolecules

There has been an increasing amount of attention given to the study of organic branched/multibranched dendrimeric molecular systems for nonlinear optics applications.[74–79] Owing to the compact structural layout of a dendrimer, a large number of chromophores can be packed into a small volume. The close proximity of the confined chromophores allows for strong electronic interactions. These strong interactions, combined with the structural symmetry associated with the system, result in enhanced nonlinear optical effects[80–85] and many other interesting properties.

Details of the excited-state formation and excitation transfer in these symmetrically branched molecular systems took some time to be clearly understood. Studies using transient absorption, time-resolved fluorescence, transient grating, and steady-state spectroscopy on dendrimeric systems characterized the excited-state dynamics.[86–89] However, these spectroscopic methods probe the population dynamics of the excited state. As a result it is difficult to gain direct information on the migration of the excitation energy and to gain a full understanding of the linear and nonlinear optical response of the system. Hence, Varnavski et al.[90] set out to investigate the excited-state dynamics of a branched donor–acceptor macromolecular system (possessing C_3 symmetry in the ground state and exhibiting charge-transfer character of the excited state) and a linear molecule representing the building block of the dendrimeric system. They used the 3PEPS method in combination with time-resolved fluorescence anisotropy and transient absorption.

Their 3PEPS results, for the branched system and the linear building block, highlighted three main features of interest. Firstly, the data revealed a large initial fast-decay component during the first 100 fs for the branched system compared to the linear building block, suggesting a different kind of initial excitation for the branched system. In conjunction with the time-resolved fluorescence, they suggested that this fast component corresponds to a delocalized state of the initial excitation in the branched system. Secondly, the higher initial peak-shift value obtained for the branched molecule suggests a smaller total coupling of the system's electronic transition to the bath. It is known from other work that a delocalized excited state over several chromophores results in a lower electron–phonon coupling compared to that of a single chromophore (due to motional narrowing effects), hence the peak-shift values obtained therein[90] seemed to be in agreement with this theory. Lastly, a nonzero asymptotic peak shift at long population times was observed and construed as residual static inhomogeneity in the system associated with the various structural conformations possible for the localization of the intramolecular charge-transfer processes within the system.

In summary, it was established that excitation in these branched systems initially goes through an intermediate delocalized excited state before the excitation is stabilized by localization onto one of the branches (breaking the molecular symmetry). The 3PEPS technique in conjunction with time-resolved fluorescence and transient absorption data were found to be

useful in probing the dynamics of energy redistribution and charge-transfer stabilization.

4.4. Single-Walled Carbon Nanotubes (SWNTs)

A common difficulty associated with the spectroscopy of SWNTs is that samples currently available have a considerable degree of heterogeneity due to various factors, including different tube types, diameter distribution, length, curvature, occurrence of defects, surfactant coating, and differences in tube environments.[91–100] Consequently, a large amount of variance in the transition frequency of a given excitation exists. Extraction of the intrinsic, homogeneous linewidth from linear spectroscopy is not feasible due to the technique's inability to resolve early-time ultrafast dynamics, hence it is ineffective in discerning the line-broadening mechanisms (i.e. fluctuations in the transition frequencies, leading to homogenous broadening, and static distributions, resulting in inhomogeneous broadening). Thus, Graham et al.[101] made use of the 3PEPS measurement to elucidate the spectral line broadening of semiconducting SWNTs in an aqueous solution and embedded in a polymer matrix.

In their investigation, Graham et al. obtained 3PEPS results that were basically indistinguishable between the two different media (i.e. the aqueous suspension and the polymer film). Due to the similarity between the results, two qualitative inferences were made regarding this observation. Firstly, the dynamics measured seemed to be insensitive to the surrounding environment of the nanotubes. Secondly, additional spectral linewidth broadening did not result from suspending the SWNTs into films (suggesting the absence of substantial tube aggregation), which would have caused an increase in asymptotic peak shift in comparison with the aqueous suspension. A strong dependence of the peak shift on the excitation intensity was found. Peak-shift data for a given sample were shifted to higher values with decreasing excitation intensity, but the 3PEPS decay profiles themselves, besides the observed shifts, were largely unaffected by intensity effects and could be overlayed after subtracting the shifts. This power-dependence was attributed to exciton–exciton scattering and annihilation. To resolve the complications involved with multiphoton absorption and extract the absorption line shape information, the 3PEPS profile in the limit of zero-intensity was constructed. Simulations were carried out where $M(t)$ was constructed, and peak shift and absorption spectrum were reproduced.

From their results, they were able to extract an initial peak-shift value of 50 fs, a decay of 60 fs, an inhomogeneous broadening width of 698 cm^{-1}, and a homogeneous width of 178 cm^{-1}. The rather high initial peak value indicates a weak system–bath coupling, the decay time constant seemed to be much shorter than the typical inertial response of the solvent, suggesting a different mechanism for the relaxation of the exciton population, and from the values of the linewidth it was concluded that the lowest allowed excitonic transition of the bulk tube species was dominated by inhomogeneous broadening (and had a narrow homogeneous width). In their investigation, through 3PEPS spectroscopy, they were able to obtain information to clearly distinguish between homogeneous and inhomogeneous broadening contributions directly on ensemble measurements and to acquire a deconvoluted spectroscopic characterization of SWNT.

5. How 3PEPS Relates to 2DPE Spectroscopy

Each of the studies of complex molecular systems described above provides insights which have demonstrated the efficacy of 3PEPS spectroscopy and have also led to discoveries concerning the interactions and dynamics in the system.

A newer generation of photon-echo spectroscopy, two-dimensional photon-echo spectroscopy (2DPE), has been under development[102–108] for over a decade and has gained popularity in the past several years. The development of the technique was inspired by 2D nuclear magnetic resonance (NMR) experiments, then later extended into infrared spectroscopy for directly probing molecular vibrations.[109–112] Currently, many of the protocols have been extended and adapted for use in the optical frequency regime to obtain ultrafast electronic dynamics and structural information after electronic excitation. Difficulties regarding rigorous phase-stability requirements and interferometric signal detection had to be overcome. The convenience of phase matching desired signals, which allows for background-free detection is also often advantageous.

3PEPS and 2DPE are the main techniques that can resolve interactions that are hidden under broad linewidths, quantify the ultrafast timescales of molecular relaxation, and thereby expose the fundamental properties of the system. 2DPE measures the system's polarization evolution (or more generally, the third-order optical response) which contains dynamic population and coherence information about the ensemble. This information, in turn, provides characterization of couplings between absorption features. Hence, the 2D plot allows for a direct visual mapping of the energetic and dynamic progression of the system's response to excitation. 2DPE offers the same nature of information as 3PEPS and beyond in a perceptive graphical manner, making it the most versatile photon-echo technique currently available.

In general, a 2DPE experiment is set up[113] and measurements are taken in a similar way to a 3PEPS experiment (Figure 6). However, the three beams are aligned to form three corners of a square and the signal is measured in only one phase-matched direction, $-\mathbf{k_1}+\mathbf{k_2}+\mathbf{k_3}$, which forms the fourth corner. Like 3PEPS, the photon-echo signal is, once again, measured while a sweep of the coherence time (from $-\tau$ to τ) is made for a fixed value of the population time (T). This procedure is repeated several times until a set of data can be collected for increasing values of T to obtain an evolution of the spectrum, hence mapping the dynamics.

Besides the variation in beam geometry, the main difference lies in the signal detection. 2DPE makes use of a fourth, local oscillator pulse which interferes with the signal to give an interferogram (heterodyne signal) detected by a charge-couple device (CCD).[105] Unlike the 3PEPS signal collection, where a detector/diode measures only the intensity of a homodyne signal, both the amplitude and phase information of the 2DPE

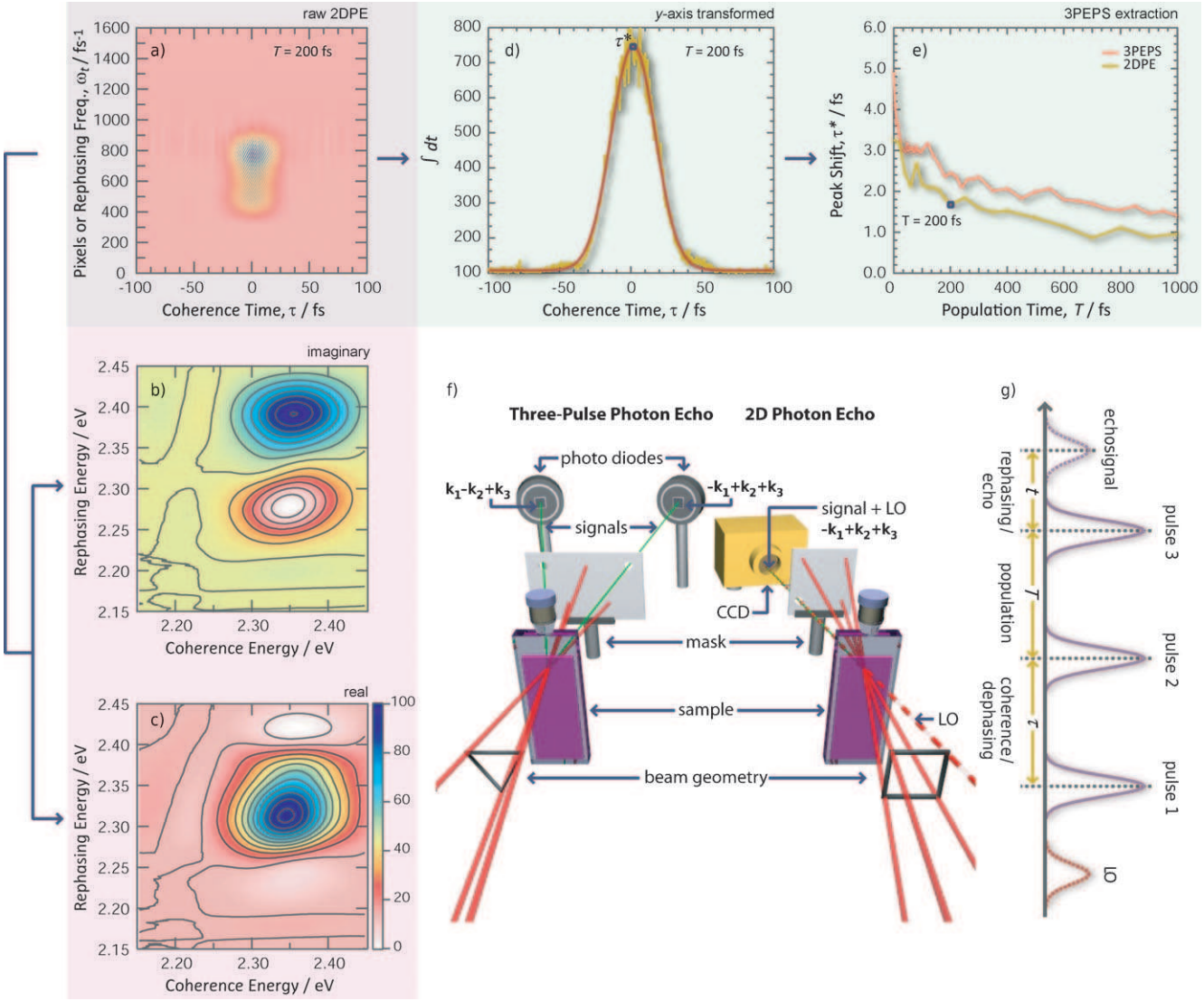

Figure 6. a)–e) 2D photon-echo data and 3PEPS extraction from Rhodamine 6G in ethanol. a)–c) From the raw 2DPE signal (a) picked up by the CCD camera at a particular population time (*T*), using the phase information obtained through a pump–probe data set and through the Fourier transformation of the τ-axis, the imaginary [refractive medium] (b) and the real [absorptive] (c) contributions of the collected signal can be separated, for which the real component is shown only in a typical 2DPE spectrum. d), e) From the same raw 2DPE signal in (a), it is possible to extract 3PEPS data by inverse Fourier transforming (IFT) the pixel axis, then integrating over the positive portion of the IFT results, which is fit to a Gaussian (giving the same integrated photon-echo profiles collected by a 3PEPS experiment), and the maxium peak-shift value (τ^*) is obtained (d). The steps are then repeated at various *T* to reconstruct the 3PEPS data set (e). f) Experimental configuration for three-pulse photon-echo peak shift and 2D photon-echo spectroscopy. In both cases, three pulses are focused on a sample, in the different beam geometries, and the photon-echo signals are emitted in the phase-matched direction, $-\mathbf{k}_1+\mathbf{k}_2+\mathbf{k}_3$ and $\mathbf{k}_1-\mathbf{k}_2+\mathbf{k}_3$ for 3PEPS and $-\mathbf{k}_1+\mathbf{k}_2+\mathbf{k}_3$ for 2DPE. In the case of 2DPE experiment, there is an additional weaker local oscillator (LO) pulse used as a reference field (the technique is called spectral interferometry), which copropagates with the echo signal and allows for heterodyne detection (both the LO and the signal are of the same wavelength). For the 3PEPS experiment, due to the absence of the LO, the signal detection is said to be homodyne detected (which gives the absolute square of the signal field). g) Pulse sequence for photon-echo experiment (for both 3PEPS and 2DPE). The variable time delays are labelled between pulses. The LO pulse only applies to the 2DPE experiment.

signal electric field is recorded. The interferometric signal picked up by the CCD camera can be displayed as a 2D plot of τ versus pixel at a particular *T*, where pixels directly correspond to the echo emission frequency (ω_t) or the energy. Through the Fourier relationship (of time and frequency), the τ-axis can be transformed to form the conventional 2DPE spectrum, displayed as ω_t versus ω_τ (or converted to rephasing energy versus coherence energy). The phase information obtained (in conjunction with a spectrally resolved pump–probe data set) is used to separate the real (absorptive) and the imaginary (refractive medium) contributions of the collected signal, for which only the real portion is used in creating the standard 2DPE spectrum.

Once the 2DPE contour plots are constructed at various *T*, some of the important features to take note of are the diagonal peaks, cross peaks (or off-diagonal peaks), asymmetry of the spectrum, and the shape of the peaks. Briefly stereotyping these features, diagonal peaks correspond to the linear absorp-

tion spectra; the position and development/formation of cross-peaks and asymmetry correspond generally to dynamics of excitation which can reveal information regarding the origin and evolution of the excitation (e.g. energy transfer, coherence, etc.). The shapes of the peaks correspond to the distribution of environments (e.g. homogeneous and inhomogeneous factors).

It is also possible to extract 3PEPS data from the 2DPE results (Figure 6). From the raw 2D plot of τ versus pixel at a particular *T*, obtained from the CCD, instead of Fourier transforming the τ-axis to obtain the conventional 2DPE spectrum, the pixel axis can be transformed to obtain the peak shift (maximum τ value, τ^*) at the particular *T*. The peak-shift values for the various *T* times can be collected and plotted as a conventional peak-shift decay, τ^* versus *T*.

In Figure 6, starting from the raw 2D photon-echo data of R6G in ethanol at $T = 200$ fs (Figure 6a), a progression of the 3PEPS extraction process is illustrated and compared with the actual 3PEPS data for R6G (Figure 6a,d,e). Furthermore, the imaginary and real (standard 2DPE plot) contributions of the collected 2D photon-echo signal are shown (Figure 6b,c). Figure 6f shows the experimental configuration for 3PEPS and 2DPE spectroscopy. Lastly, the pulse sequence for both photon-echo experiments can be seen in Figure 6g, keeping in mind that the LO pulse only applies to the 2DPE experiment.

2DPE offers an abundant amount of information, from the linear absorption spectrum, couplings between electronic interactions, energy migration, coherence dynamics, to bath–system interactions (including 3PEPS data), even for the most convoluted systems.[71,114–118] The information is all contained within the 2D data obtained, but a suitable form of data reduction must be applied in order to extract the information that is desired.

6. Conclusions

Spectroscopic studies of condensed-phase multichromophoric systems are convoluted by solute–solvent interactions occuring over a wide range of timescales. To better understand chemical reactivity, information regarding the system–bath interactions and dynamics are essential. 3PEPS spectroscopy allows us to investigate these environmental fluctuations around a chromophore. Herein, we described how 3PEPS works, reviewed recent 3PEPS applications involving complex multichromophoric systems, and showed how 3PEPS data can be extracted from 2D photon-echo data. The 2D visualization of information in 2DPE often allows a more intuitive way to resolve complex dynamics occurring in systems and allows for the identification of phenomena that cannot be measured using other forms of spectroscopy.[71,114] 3PEPS measurements have been the preferred, simplistic, and direct method for obtaining solvation correlation functions, which allows for the determination of the spectral density relevant to the solvation process. However, the direct physical interpretation of the 3PEPS results is not always an intuitive process and requires careful consideration, in combination with modeling and other types of experiments. The extraction of this useful 3PEPS data from 2DPE results emphasizes the versatility of 2DPE spectroscopy and its power to characterize diverse and complex molecular systems.

Acknowledgements

The Natural Science and Engineering Research Council is gratefully acknowledged for the support of this research.

Keywords: condensed phase · chromophores · nonlinear optics · laser spectroscopy · ultrafast solvation dynamics

[1] S. F. Mason, *J. Chem. Soc.* **1959**, 1263 – 1268.
[2] Y. Ooshika, *J. Phys. Soc. Jpn.* **1954**, *9*, 594 – 602.
[3] E. G. McRae, *J. Phys. Chem.* **1957**, *61*, 562 – 572.
[4] a) N. Mataga, Y. Kaifu, M. Koizumi, *Bull. Chem. Soc. Jpn.* **1956**, *29*, 465 – 470; b) N. Mataga, *Bull. Chem. Soc. Jpn.* **1963**, *36*, 654 – 662.
[5] E. Lippert, *Z. Naturforsch. A* **1955**, *10*, 541 – 545.
[6] P. Suppan, *J. Photochem. Photobiol. A* **1990**, *50*, 293 – 330.
[7] a) J. Tomasi, M. Persico, *Chem. Rev.* **1994**, *94*, 2027 – 2094; b) J. Tomasi, B. Mennucci, R. Cammi, *Chem. Rev.* **2005**, *105*, 2999 – 3094.
[8] C. J. Cramer, D. G. Truhlar, *Chem. Rev.* **1999**, *99*, 2161 – 2200.
[9] C. Reichardt, *Chem. Rev.* **1994**, *94*, 2319 – 2358.
[10] a) R. A. Marcus, *J. Chem. Phys.* **1963**, *39*, 1734 – 1740; b) R. A. Marcus, *J. Chem. Phys.* **1965**, *43*, 1261 – 1274.
[11] M. Orrit, J. Bernard, R. I. Personov, *J. Phys. Chem.* **1993**, *97*, 10256 – 10268.
[12] R. Jankowiak, J. M. Hayes, G. J. Small, *Chem. Rev.* **1993**, *93*, 1471 – 1502.
[13] W. E. Moerner, *J. Phys. Chem. B* **2002**, *106*, 910 – 927.
[14] S. Mukamel, *Principles of Nonlinear Optical Spectroscopy*, Oxford University Press, New York, **1995**.
[15] a) G. R. Fleming, S. A. Passino, Y. Nagasawa, *Philos. Trans. R. Soc. Lond. A* **1998**, *356*, 389 – 404; b) G. R. Fleming, M. Cho, *Annu. Rev. Phys. Chem.* **1996**, *47*, 109 – 134.
[16] B. Bagchi, D. Oxtoby, G. Fleming, *Chem. Phys.* **1984**, *86*, 257 – 267.
[17] G. van der Zwan, J. T. Hynes, *J. Phys. Chem.* **1985**, *89*, 4181 – 4188.
[18] a) T. Joo, Y. Jia, J.-Y. Yu, M. J. Lang, G. R. Fleming, *J. Chem. Phys.* **1996**, *104*, 6089 – 6107; b) T. Joo, Y. Jia, J.-Y. Yu, D. M. Jonas, G. R. Fleming, *J. Phys. Chem.* **1996**, *100*, 2399 – 2409.
[19] D. M. Jonas, M. J. Lang, Y. Nagasawa, T. Joo, G. R. Fleming, *J. Phys. Chem.* **1996**, *100*, 12660 – 12673.
[20] M. Cho, *Two-Dimensional Optical Spectroscopy*, CRC Press, Boca Raton, **2009**.
[21] E. W. Castner Jr. , M. Maroncelli, G. R. Fleming, *J. Chem. Phys.* **1987**, *86*, 1090 – 1097.
[22] M. Maroncelli, G. R. Fleming, *J. Chem. Phys.* **1987**, *86*, 6221 – 6239.
[23] M. L. Horng, J. A. Gardecki, M. Maroncelli, *J. Phys. Chem.* **1995**, *99*, 17311 – 17337.
[24] a) B. M. Ladanyi, R. M. Stratt, *J. Phys. Chem.* **1996**, *100*, 1266 – 1282; b) B. M. Ladanyi, R. M. Stratt, *J. Phys. Chem.* **1995**, *99*, 2502 – 2511.
[25] B. Mennucci, R. Cammi, *Continuum Solvation Models in Chemical Physics, From Theory to Applications*, Wiley, Chichester, **2007**.
[26] a) J. Tomasi, B. Mennucci, R. Cammi, *Chem. Rev.* **2005**, *105*, 2999 – 3093; b) J. Tomasi, R. Cammi, B. Mennucci, C. Cappelli, S. Corni, *Phys. Chem. Chem. Phys.* **2002**, *4*, 5697 – 5712.
[27] M. Maroncelli, *J. Mol. Liq.* **1993**, *57*, 1 – 37.
[28] R. M. Stratt, M. Maroncelli, *J. Phys. Chem.* **1996**, *100*, 12981 – 12996.
[29] P. J. Rossky, J. D. Simon, *Nature* **1994**, *370*, 263 – 269.
[30] W. Jarzeba, G. C. Walker, A. E. Johnson, P. F. Barbara, *Chem. Phys.* **1991**, *152*, 57 – 68.
[31] P. F. Barbara, W. Jarzeba, *Adv. Photochem.* **1990**, *15*, 1 – 68.
[32] R. Kubo, *Rep. Prog. Phys.* **1966**, *29*, 255 – 284.
[33] M. Maroncelli, G. R. Fleming, *J. Chem. Phys.* **1988**, *89*, 875 – 881.
[34] S. J. Rosenthal, X. Die, M. Du, G. R. Fleming, *J. Chem. Phys.* **1991**, *95*, 4715 – 4718.
[35] R. Jimenez, G. R. Fleming, P. V. Kumar, M. Maroncelli, *Nature* **1994**, *369*, 471 – 473.

[36] M. Maroncelli, P. V. Kumar, A. Papazyan, M. L. Horng, S. J. Rosenthal, G. R. Fleming, *Ultrafast Reaction Dynamics and Solvent Effects* in *AIP Conf. Proc*. (Eds.: Y. Gauduel, P. J. Rossky), **1994**, *298*, 310 – 333.
[37] E. A. Carter, J. T. Hynes, *J. Chem. Phys.* **1991**, *94*, 5961 – 5979.
[38] R. M. Stratt, *Acc. Chem. Res.* **1995**, *28*, 201 – 207.
[39] B. J. Schwartz, P. J. Rossky, *J. Phys. Chem.* **1995**, *99*, 2953 – 2958.
[40] a) W. P. de Boeij, M. S. Pshenichnikov, D. A. Wiersma, *J. Phys. Chem.* **1996**, *100*, 11806 – 11823; b) W. P. de Boeij, M. S. Pshenichnikov, D. A. Wiersma, *Chem. Phys. Lett.* **1996**, *253*, 53 – 60.
[41] T. Joo, Y. Jia, G. R. Fleming, *J. Chem. Phys.* **1995**, *102*, 4063 – 4068.
[42] T. E. Dykstra, *Photophysics of Conjugated Polymers*, unpublished Ph.D. thesis, University of Toronto, **2008**.
[43] M. Cho, J.-Y. Yu, T. Joo, Y. Nagasawa, S. A. Passino, G. R. Fleming, *J. Phys. Chem.* **1996**, *100*, 11944 – 11953.
[44] M. R. Salvador, P. S. Nair, M. Cho, G. D. Scholes, *Chem. Phys.* **2008**, *350*, 56 – 68.
[45] G. D. Scholes, D. S. Larsen, G. R. Fleming, G. Rumbles, P. L. Burn, *Phys. Rev. B* **2000**, *61*, 13670 – 13678.
[46] M. Yang, *Chem. Phys. Lett.* **2009**, *467*, 304 – 308.
[47] K. F. Everitt, E. Geva, J. L. Skinner, *J. Chem. Phys.* **2001**, *114*, 1326 – 1335.
[48] S. A. Passino, Y. Nagasawa, T. Joo, G. R. Fleming, *J. Phys. Chem. A* **1997**, *101*, 725 – 731.
[49] Y. Nagasawa, J.-Y. Yu, G. R. Fleming, *J. Chem. Phys.* **1998**, *109*, 6175 – 6183.
[50] D. S. Larsen, K. Ohta, G. R. Fleming, *J. Chem. Phys.* **1999**, *111*, 8970 – 8979.
[51] A. Piryatinski, C. P. Lawrence, J. L. Skinner, *J. Chem. Phys.* **2003**, *118*, 9672 – 9679.
[52] a) D. S. Larsen, K. Ohta, Q.-H. Xu, M. Cyrier, G. R. Fleming, *J. Chem. Phys.* **2001**, *114*, 8008 – 8039; b) D. S. Larsen, *Rev. Sci. Instrum.* **2002**, *73*, 1325 – 1328.
[53] R. Agarwal, B. S. Prall, A. H. Rizvi, M. Yang, G. R. Fleming, *J. Chem. Phys.* **2002**, *116*, 6243 – 6252.
[54] J. M. Salverda, M. Vengris, B. P. Krueger, G. D. Scholes, A. R. Czarnoleski, V. Novoderezhkin, H. van Amerongen, R. van Grondelle, *Biophys. J.* **2003**, *84*, 450 – 465.
[55] S. M. Gallagher Faeder, D. M. Jonas, *Phys. Rev. A* **2000**, *62*, 033820.
[56] M. R. Salvador, M. A. Hines, G. D. Scholes, *J. Chem. Phys.* **2003**, *118*, 9380 – 9388.
[57] L. J. McKimmie, C. N. Lincoln, J. Jasieniak, T. A. Smith, *J. Phys. Chem. C* **2010**, *114*, 82 – 88.
[58] X. Yang, T. E. Dykstra, G. D. Scholes, *Phys. Rev. B* **2005**, *71*, 045203.
[59] T. E. Dykstra, V. Kovalevskij, X. Yang, G. D. Scholes, *Chem. Phys.* **2005**, *318*, 21 – 32.
[60] T. E. Dykstra, G. D. Scholes in *Conformational Disorder and Optical Properties of Conjugated Polymers: Ultrafast Dynamics and Laser Action of Organic Semiconductors* (Ed. Z. V. Vardeny), CRC Press, Boca Raton, **2009**.
[61] S. Tretiak, A. Saxena, R. L. Martin, A. R. Bishop, *Phys. Rev. Lett.* **2002**, *89*, 097402.
[62] J. Bullot, B. Dulieu, S. Lefrant, *Synth. Met.* **1993**, *61*, 211 – 215.
[63] G. R. Möhlmann, *Synth. Met.* **1994**, *67*, 77 – 80.
[64] D. R. Baigent, N. C. Greenham, J. Grüner, R. N. Marks, R. H. Friend, R. C. Moratti, A. B. Holmes, *Synth. Met.* **1994**, *67*, 3 – 10.
[65] D. Oelkrug, A. Tompert, H.-J. Egelhaaf, M. Hanack, E. Steinhuber, M. Hohloch, H. Meier, U. Stalmach, *Synth. Met.* **1996**, *83*, 231 – 237.
[66] H.-J. Egelhaaf, L. Lüer, A. Tompert, P. Bäuerle, K. Müllen, D. Oelkrug, *Synth. Met.* **2000**, *115*, 63 – 68.
[67] E. Birckner, U. W. Grimmt, A. Hartmann, S. Pfeiffer, H. Tillmann H.-H. Hörhold, *J. Fluoresc.* **1998**, *8*, 73 – 80.
[68] D. Oelkrug, A. Tompert, J. Gierschner, H.-J. Egelhaaf, M. Hanack, M. Hohloch, E. Steinhuber, *J. Phys. Chem. B* **1998**, *102*, 1902 – 1907.
[69] K. P. Fritz, G. D. Scholes, *J. Phys. Chem. B* **2003**, *107*, 10141 – 10147.
[70] S. Son, A. Dodabalapur, A. J. Lovinger, M. E. Galvin, *Science* **1995**, *269*, 376 – 378.
[71] a) E. Collini, C. Y. Wong, K. E. Wilk, P. M. G. Curmi, P. Brumer, G. D. Scholes, *Nature* **2010**, *463*, 644; b) E. Collini, G. D. Scholes, *J. Phys. Chem. A* **2009**, *113*, 4223 – 4241.
[72] N. P. Wells, D. A. Blank, *Phys. Rev. Lett.* **2008**, *100*, 086403.
[73] M. Yang, G. R. Fleming, *J. Chem. Phys.* **1999**, *110*, 2983 – 2990.
[74] R. Kopelman, M. Shortreed, Z. Y. Shi, W. H. Tan, Z. F. Xu, J. S. Moore, A. Bar-Haim, J. Klafter, *Phys. Rev. Lett.* **1997**, *78*, 1239 – 1242.
[75] A. Bar-Haim, J. Klafter, R. Kopelman, *J. Am. Chem. Soc.* **1997**, *119*, 6197 – 6198.
[76] O. Varnavski, I. D. W. Samuel, L.-O. Pålsson, R. Beavington, P. L. Burn, T. Goodson III, *J. Chem. Phys.* **2002**, *116*, 8893 – 8903.
[77] J. P. J. Markham, S.-C. Lo, S. W. Magennis, P. L. Burn, I. D. W. Samuel, *Appl. Phys. Lett.* **2002**, *80*, 2645 – 2647.
[78] J. M. Lupton, I. D. W. Samuel, R. Beavington, P. L. Burn, H. Bassler, *Synth. Met.* **2001**, *116*, 357 – 362.
[79] C. W. Tang, S. A. Van Slyke, C. H. Chen, *J. Appl. Phys.* **1989**, *65*, 3610 – 3616.
[80] S. Brasselet, J. Zyss, *J. Opt. Soc. Am. B* **1998**, *15*, 257 – 288.
[81] T. Verbiest, K. Clays, C. Samyn, J. Wolff, D. Reinhoudt, A. Persoon, *J. Am. Chem. Soc.* **1994**, *116*, 9320 – 9323.
[82] S.-J. Chung, K.-S. Kim, T.-C. Lin, G.-S. He, J. Swiatkiewicz, P. N. Prasad, *J. Phys. Chem. B* **1999**, *103*, 10741 – 10745.
[83] M. Drobizhev, A. Karotki, A. Rebane, *Opt. Lett.* **2001**, *26*, 1081 – 1083.
[84] S. A. Lahankar, R. West, O. Varnavski, X. Xie, L. Sukhomlinova, R. Twieg, T. Goodson III, *J. Chem. Phys.* **2004**, *120*, 337 – 344.
[85] O. Varnavski, A. Leanov, L. Liu, J. Takacs, T. Goodson III, *J. Phys. Chem. B* **2000**, *104*, 179 – 188.
[86] L. Latterini, G. De Belder, G. Schweitzer, M. Van der Auweraer, F. C. De Schryver, *Chem. Phys. Lett.* **1998**, *295*, 11 – 16..
[87] W. Verbouwe, M. Van der Auweraer, F. C. De Schryver, J. J. Piet, J. M. Warman, *J. Am. Chem. Soc.* **1998**, *120*, 1319 – 1324.
[88] E. van Veldhoven, H. Zhang, M. Glasbeek, *J. Phys. Chem. A* **2001**, *105*, 1687 – 1692.
[89] A. Curioni, M. Boero, W. Andreoni, *Chem. Phys. Lett.* **1998**, *294*, 263 – 271.
[90] O. Varnavski, L. Sukhomlinova, R. Twieg, T. Goodson III, *J. Phys. Chem. B* **2004**, *108*, 10484 – 10492.
[91] S. M. Bachilo, M. S. Strano, C. Kittrell, R. H. Hauge, R. E. Smalley, R. B. Weisman, *Science* **2002**, *298*, 2361 – 2366.
[92] F. Wang, G. Dukovic, L. E. Brus, T. F. Heinz, *Science* **2005**, *308*, 838 – 841.
[93] Y.-Z. Ma, L. Valkunas, S. M. Bachilo, G. R. Fleming, *J. Phys. Chem. B* **2005**, *109*, 15671 – 15674.
[94] Y.-Z. Ma, T. Hertel, Z. V. Vardeny, G. R. Fleming, L. Valkunas, *Topics in Applied Physics* (Eds.: A. Jorio, G. Dresselhaus, M. S. Dresselhaus), **2008**, *111*, 321 – 352.
[95] S. M. Bachilo, L. Balzano, J. E. Herrera, F. Pompeo, D. E. Resasco, R. B. Weisman, *J. Am. Chem. Soc.* **2003**, *125*, 11186 – 11187.
[96] S. Lebedkin, P. Schweiss, B. Renker, S. Malik, F. Hennrich, M. Neumaier, C. Stoermer, M. M. Kappes, *Carbon* **2002**, *40*, 417 – 423.
[97] Y. Miyauchi, S. Chiashi, Y. Murakami, Y. Hayashida, S. Maruyama, *Chem. Phys. Lett.* **2004**, *387*, 198 – 203.
[98] A. Hagen, M. Steiner, M. B. Raschke, C. Lienau, T. Hertel, H. Qian, A. J. Meixner, A. Hartschuh, *Phys. Rev. Lett.* **2005**, *95*, 197401.
[99] J. Lefebvre, D. G. Austing, J. Bond, P. Finnie, *Nano Lett.* **2006**, *6*, 1603 – 1608.
[100] H. Htoon, M. J. O'Connell, P. J. Cox, S. K. Doorn, V. Klimov, *Phys. Rev. Lett.* **2004**, *93*, 027401.
[101] M. W. Graham, Y.-Z. Ma, G. R. Fleming, *Nano Lett.* **2008**, *8*, 3936 – 3941.
[102] a) M. Cho, T. Brixner, I. V. Stiopkin, H. M. Vaswani, G. R. Fleming, *J. Chin. Chem. Soc.* **2006**, *53*, 15 – 24; b) M. Cho, *Chem. Rev.* **2008**, *108*, 1331 – 1418.
[103] G. D. Goodno, V. Astinov, R. J. D. Miller, *J. Phys. Chem. B* **1999**, *103*, 603 – 607.
[104] J. P. Ogilvie, M. L. Cowan, R. J. D. Miller in *Diffractive Optics-Based Heterodyne Detected Three-Pulse Photon-Echo, Ultrafast Phenomena XIII* (Eds.: R. J. D. Miller, M. M. Murnane, N. F. Scherer, A. M. Weiner), Springer-Verlag, Berlin, **2003**.
[105] a) L. Lepetit, M. Joffre, *Opt. Lett.* **1996**, *21*, 564 – 566; b) L. Lepetit, G. Cheriaux, M. Joffre, *J. Opt. Soc. Am. B* **1995**, *12*, 2467 – 2474.
[106] D. M. Jonas, *Annu. Rev. Phys. Chem.* **2003**, *54*, 425 – 463.
[107] a) T. Brixner, I. V. Stiopkin, G. R. Fleming, *Opt. Lett.* **2004**, *29*, 884 – 886; b) T. Brixner, T. Mancal, I. V. Stiopkin, G. R. Fleming, *J. Chem. Phys.* **2004**, *121*, 4221 – 4236.
[108] M. L. Cowan, J. P. Ogilvie, R. J. D. Miller, *Chem. Phys. Lett.* **2004**, *386*, 184 – 189.

[109] N. S. Ginsberg, Y.-C. Cheng, G. R. Fleming, *Acc. Chem. Res.* **2009**, *42*, 1352 – 1363.
[110] R. R. Ernst, G. Bodenhausen, A. Wokaun, *Principles of Nuclear Magnetic Resonance in One and Two Dimensions*, Oxford University Press, Oxford, **1990**.
[111] P. Hamm, M. Lim, R. M. Hochstrasser, *J. Phys. Chem. B* **1998**, *102*, 6123 – 6138.
[112] Z. Ganim, H. S. Chung, A. W. Smith, L. P. DeFlores, K. C. Jones, A. Tokmakoff, *Acc. Chem. Res.* **2008**, *41*, 432 – 441.
[113] T. Brixner, J. Stenger, H. M. Vaswani, M. Cho, R. E. Blankenship, G. R. Fleming, *Nature* **2005**, *434*, 625 – 658.
[114] G. S. Engel, T. R. Calhoun, E. L. Read, T. K. Ahn, T. Mancal, Y.-C. Cheng, R. E. Blankenship, G. R. Fleming, *Nature* **2007**, *446*, 782 – 786.
[115] D. Abramavicius, B. Palmieri, D. V. Voronine, F. Sanda, S. Mukamel, *Chem. Rev.* **2009**, *109*, 2350 – 2408.
[116] T. R. Calhoun, N. S. Ginsberg, G. S. Schlau-Cohen, Y.-C. Cheng, M. Ballottari, R. Bassi, G. R. Fleming, *J. Phys. Chem. B* **2009**, *113*, 16291 – 16295.
[117] F. Milota, J. Sperling, A. Nemeth, T. Mancal, H. F. Kauffmann, *Acc. Chem. Res.* **2009**, *42*, 1364 – 1374.
[118] S. T. Cundiff, T. H. Zhang, A. D. Bristow, D. Karaiskaj, X. C. Dai, *Acc. Chem. Res.* **2009**, *42*, 1423 – 1432.

Received: September 1, 2010
Published online on November 10, 2010

